ARTICLE

doi:10.1038/nature10337

Lgr5 homologues associate with Wnt receptors and mediate R-spondin signalling

Wim de Lau[1]*, Nick Barker[1]†*, Teck Y. Low[2], Bon-Kyoung Koo[1], Vivian S. W. Li[1], Hans Teunissen[1], Pekka Kujala[3], Andrea Haegebarth[1]†, Peter J. Peters[3], Marc van de Wetering[1], Daniel E. Stange[1], Johan E. van Es[1], Daniele Guardavaccaro[1], Richard B. M. Schasfoort[4], Yasuaki Mohri[5], Katsuhiko Nishimori[5], Shabaz Mohammed[2], Albert J. R. Heck[2] & Hans Clevers[1]

The adult stem cell marker Lgr5 and its relative Lgr4 are often co-expressed in Wnt-driven proliferative compartments. We find that conditional deletion of both genes in the mouse gut impairs Wnt target gene expression and results in the rapid demise of intestinal crypts, thus phenocopying Wnt pathway inhibition. Mass spectrometry demonstrates that Lgr4 and Lgr5 associate with the Frizzled/Lrp Wnt receptor complex. Each of the four R-spondins, secreted Wnt pathway agonists, can bind to Lgr4, -5 and -6. In HEK293 cells, RSPO1 enhances canonical WNT signals initiated by WNT3A. Removal of LGR4 does not affect WNT3A signalling, but abrogates the RSPO1-mediated signal enhancement, a phenomenon rescued by re-expression of LGR4, -5 or -6. Genetic deletion of *Lgr4/5* in mouse intestinal crypt cultures phenocopies withdrawal of Rspo1 and can be rescued by Wnt pathway activation. Lgr5 homologues are facultative Wnt receptor components that mediate Wnt signal enhancement by soluble R-spondin proteins. These results will guide future studies towards the application of R-spondins for regenerative purposes of tissues expressing Lgr5 homologues.

The genes *Lgr4*, *Lgr5* and *Lgr6* encode orphan 7-transmembrane receptors that are close relatives of the receptors for follicle stimulating hormone (FSH), luteinizing hormone (LH) and thyroid-stimulating hormone (TSH)[1]. It is currently unknown how they signal and what their ligands are. *Lgr5* is a Wnt target gene that marks proliferative stem cells in several Wnt-dependent stem cell compartments, that is, the small intestine and colon[2], the stomach[3] and the hair follicle[4]. *Lgr6* marks multipotent stem cells in the epidermis[5]. The expression of *Lgr4* is much broader[6], but we noted that *Lgr5* is co-expressed with *Lgr4* in the stem cell compartments mentioned above. For instance, *Lgr5* marks small intestinal stem cells at the crypt base, whereas *Lgr4* marks all crypt cells, including $Lgr5^+$ stem cells (Fig. 1a). The same observation was made in ref. 7. Indeed, our previously reported microarray study, which compared $Lgr5^+$ stem cells to their immediate daughters, showed that *Lgr4* is expressed in both cell types[8]. Moreover, we generated an allele of *Lgr4* in which a green fluorescent protein-internal ribosomal entry site-CreERT2 (GFP-IRES-CreERT2) cassette was inserted into the ATG start codon, as performed previously for *Lgr5* (ref. 2) and *Lgr6* (ref. 5). Tamoxifen-induced lineage tracing after crossing to the R26R-LacZ Cre reporter strain demonstrated that *Lgr4* is expressed both by short-lived progenitors and by long-lived stem cells (Supplementary Fig. 1). Of note, *Lgr4* and *Lgr5* null mutations are neonatal-lethal in mice[9,10].

To address a potential function in crypts, we generated an $Lgr5^{fl}$ allele (Supplementary Fig. 2a) by flanking exon 16 with *loxp* sites; its deletion causes a frame shift. This allele was crossed into a mouse strain carrying conditional $Lgr4^{fx}$ alleles[10] and the gut-specific *Ah-Cre* transgene, which is inducible by β-naphtoflavone[11]. Conditional deletion of *Lgr5* alone in the intestinal epithelium of adult mice yielded no apparent phenotype, and did not confirm the Paneth cell phenotype reported previously in *Lgr5* null neonatal mice[12]. Deletion of *Lgr4* alone induced loss of proliferation and crypt loss, obvious from day 4–5 post-induction onwards. Paneth cells at crypt bottoms were retained in 'nests', disconnected from the surface epithelium. No direct effects were observed on differentiated cells. The combined deletion of *Lgr4* and *-5* enhanced this crypt phenotype as judged by the cell proliferation marker Ki67 and the stem cell marker olfactomedin 4 (Olfm4; ref. 13). Figure 1b and Supplementary Fig. 2b depict typical results obtained at day 5 post-induction. Of note, hyperplastic wild-type 'escaper' crypts (arrows in Fig. 1b, and see ref. 14) served as staining control. Over the next few days, villi shortened and eventually the phenotype was not compatible with life. A gut phenotypic analysis was reported recently for mice homozygous for a hypomorphic *Lgr4* allele that live for about 1 month postnatally[7]. These mice displayed twofold reduced proliferation and an 85% reduction in Paneth cells, whereas stem cell markers and Wnt target genes were unaffected *in vivo*. In 'minigut' culture[15], *Lgr4*-hypomorphic crypts failed to initiate organoid growth. No genetic interaction with an *Lgr5* null allele was observed for this intestinal phenotype.

Two signalling pathways, Wnt[16,17] and Notch[18], are crucial for the maintenance of adult crypt proliferation. We determined gene expression changes by microarraying on day 1 post-deletion of *Lgr4* and *-5*, when stem cells were physically still present (Supplementary Fig. 3). Simultaneous deletion of *Lgr4* and *Lgr5* resulted in downregulation of 306 genes in two separate experiments (*Lgr4/5* gene set; Supplementary Table 1). These included 29 stem cell-enriched genes[8]. To determine if these are Wnt target genes, we analysed this gene set in two complementary scenarios that detect intestinal Wnt target genes. In the first scenario[19], *in vivo* deletion of *Apc* results in the immediate upregulation of Wnt target genes. Comparison of the *Lgr4/5* gene set to the microarray data from ref. 19 showed a significant upregulation of 53% (137 genes) of the *Lgr4/5* gene set, whereas only 5% (12 genes) were significantly downregulated (Fig. 2a, red ratios). Indeed, gene set enrichment analysis (GSEA)[20] showed a highly significant enrichment (false

[1]Hubrecht Institute and University Medical Center Utrecht, 3584 CX Utrecht, The Netherlands. [2]Biomolecular Mass Spectrometry and Proteomics group, Bijvoet Center for Biomolecular Research and Utrecht Institute for Pharmaceutical Sciences, Utrecht University. Netherlands Proteomics Centre, Padualaan 8, 3584 CH Utrecht, The Netherlands. [3]Antoni van Leeuwenhoek Hospital Netherlands Cancer Institute, 1066 CX Amsterdam, The Netherlands. [4]Medical Cell Biophysics, MIRA institute, University of Twente, 7500 AE Enschede, The Netherlands. [5]Tohoku University, 981-8555 Sendai, Miyagi, Japan. †Present addresses: Institute of Medical Biology, 06-06 Immunos, Singapore 138648 (N.B.); Bayer Schering Pharma AG, 13353 Berlin, Germany (A.H.).
*These authors contributed equally to this work.

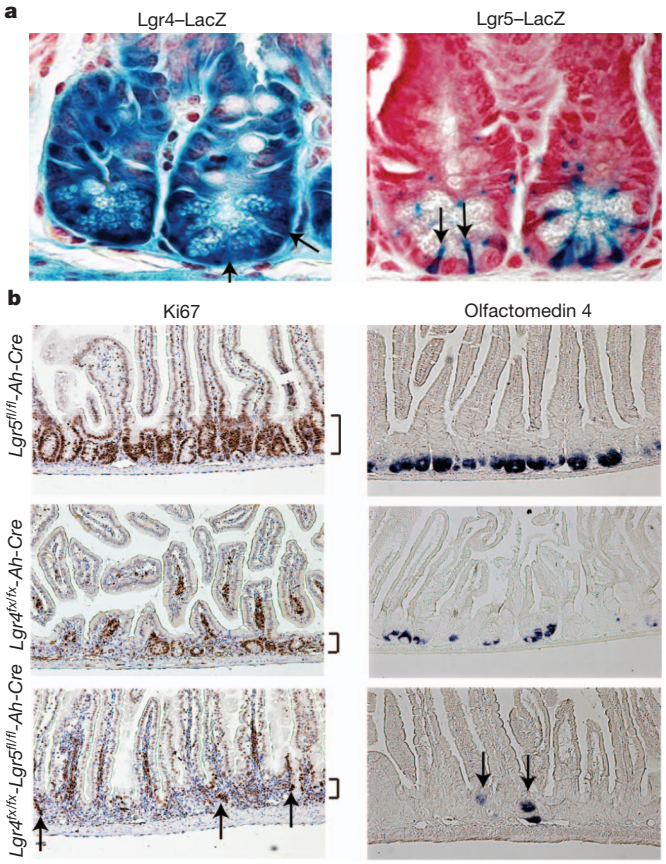

Figure 1 | Conditional deletion of *Lgr4* and *Lgr5*. **a**, Left, expression of Lgr4–lacZ[6] (blue) occurs throughout intestinal crypts. Right, expression of Lgr5–LacZ (blue) is specific to stem cells (arrows) located between Paneth cells at bottom of crypts[2]. **b**, Adult $Lgr4^{fx/fx}$ and/or $Lgr5^{fl/fl}$ mice carrying the *Ah-Cre* transgene, analysed 5 days after Cre-activation[11]. Left panels, proliferation visualized by Ki67. Vertical bars, crypt width. Right panels, stem cells visualized by *OlfM4 in situ* hybridization. Top, *Lgr5* deletion has no obvious effect. Middle, *Lgr4* deletion has significant deleterious effects on crypt stem cells and proliferative progenitors. Bottom, upon *Lgr4/5* double deletion, >80% of crypts entirely disappear. Arrows indicate wild-type escaper crypts that express OlfM4 and are $Ki67^{+}$.

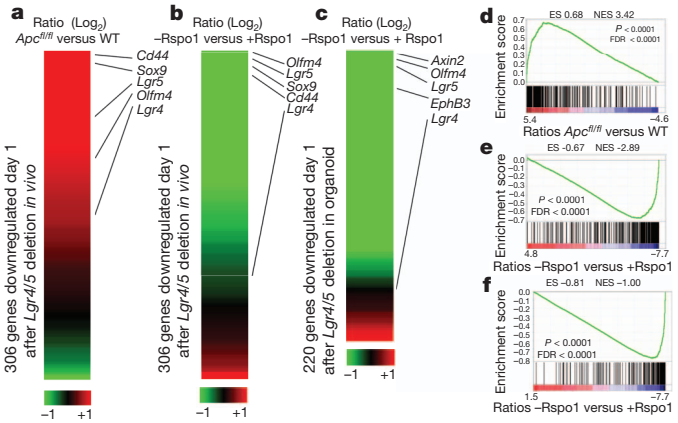

Figure 2 | Wnt target genes are downstream of Lgr4/5. Concomitant deletion of *Lgr4* and *Lgr5* in $Lgr4^{fl/fl}$ $Lgr5^{fl/fl}$ mice resulted in downregulation of 307 unique genes 1 day after deletion (Supplementary Table 1). The intestinal Wnt signature can be revealed by two opposing experiments: deletion of *Apc in vivo* results in upregulation of a Wnt target signature[19], whereas Rspo1 withdrawal from intestinal organoids[15] results in downregulation of this signature. **a**, Heat map of the $\log_2$ ratio of $Apc^{fl/fl}$ mice versus control wild-type mice (WT) for the 307 *Lgr4/5* genes 3 days after deletion of *Apc* (ratios taken from ref. 19). **b**, Heat map of the $\log_2$ ratio of intestinal organoids 1 day after Rspo1 withdrawal (−Rspo1) versus control organoids (+Rspo1) for the 307 *Lgr4/5* gene set. **c**, Heat map of the $\log_2$ ratio of intestinal organoids 1 day after Rspo1 withdrawal (−Rspo1) versus control organoids (+Rspo1) for the 220 downregulated genes in $Lgr4^{fl/fl}$ $Lgr5^{fl/fl}$ organoids (1 day after deletion). **d**, Gene set enrichment analysis (GSEA). Genes are ranked according to their differential expression between *Apc*-deleted and wild-type mice (data from ref. 19). Black bars beneath the graph depict the rank positions of the 306 genes from the *Lgr4/5* gene set. A highly significant enrichment of the 306 *Lgr4/5* genes was detected towards the gene set upregulated 3 days after *Apc* deletion *in vivo*. **e**, Genes ranked according to differential expression in intestinal organoids after Rspo1 withdrawal versus control organoids. GSEA shows a highly significant enrichment of the 306 *Lgr4/5* genes towards the genes downregulated after Rspo1 withdrawal. **f**, Genes are ranked according to their differential expression in intestinal organoids after Rspo1 withdrawal versus control organoids. GSEA shows a highly significant enrichment of the 220 *Lgr4/5* downregulated genes in organoids towards those genes downregulated after Rspo1 withdrawal. ES, enrichment score; FDR, false discovery rate; NES, normalized ES.

discovery rate (FDR) and *P*-value < 0.0001) of the *Lgr4/5* gene set towards the upregulated genes after *Apc* deletion (Fig. 2d). For the second scenario, we performed microarraying before, and 1 day after, acute withdrawal of the Wnt agonist Rspo1 from cultured small intestinal crypt organoids[15]. This resulted in the immediate down-regulation of 38% (166 genes) of the *Lgr4/5* gene set, whereas only 4% (11 genes) showed the opposite behaviour. (Fig. 2b, green ratios). GSEA analysis confirmed the highly significant enrichment (FDR and *P*-value < 0.0001) of the *Lgr4/5* gene set towards the downregulated genes after Rspo1 withdrawal (Fig. 2e).

To find molecular partners of LGR receptors, we pursued a tandem affinity purification mass spectrometric strategy. Bait proteins carried double Flag-haemagglutinin (FH)-tags[21]. First, we transiently transfected tagged Frizzled7 (Frz7–FH; frizzled family receptor 7 is also known as FZD7) into HEK293T cells. We detected significant signatures for Frizzled7, and—as expected—the WNT co-receptors LRP5 and LRP6. Surprisingly, multiple peptides were detected for LGR4 (Supplementary Table 2). Of note, we never observed LGR5 homologues, frizzled or LRP proteins in HEK293 cells using ~20 unrelated baits (Supplementary Table 3). We then generated stable clones of LS174T colorectal cancer cells that moderately overexpress tagged versions of LGR4, LGR5 or Frizzled5. The LGR4 bait captured LGR5, LRP6, Frizzled5 and Frizzled7. The LGR5 bait captured Frizzled6 and LRP5 and LRP6. The Frizzled5 bait captured LGR4, LGR5, LRP5 and LRP6. These proteins were never observed in the non-transfected controls run in parallel. Results are summarized in Supplementary Table 2. Thus, LGR4 and LGR5 can occur in a physical complex with frizzled proteins and LRP5/6.

The four secreted R-spondin proteins activate the canonical Wnt pathway and are particularly potent when synergizing with secreted Wnt proteins[22,23]. Systemic delivery of Rspo1 in mice leads to a dramatic enhancement of the Wnt-responsive intestinal crypts[24] and stimulates epithelial repair[25]. Whereas Rspo3 uses syndecans as receptors to mediate non-canonical Wnt signals[26], the R-spondin receptors that drive canonical Wnt signals have remained controversial[26]. Rspo1 was proposed to bind the Wnt co-receptor Lrp6 (refs 27, 28), to block the Kremen protein that downregulates surface expression of Wnt receptors[29], or to block the interaction of the Wnt inhibitor Dkk1 with Lrp6 (ref. 23). HEK293T cells are responsive to WNT3A and R-spondin[22]. We used this cell line to search for the cognate R-spondin receptor. To validate the efficacy of using secreted baits to detect surface receptors, we generated a tagged version of Dkk1 (Dkk1–FH). Dkk1 interacts with LRP5/6 (ref. 30). We incubated 2×10^9 HEK293T cells with Dkk1–FH. The cells were washed, lysed and immunoprecipitated with an anti-Flag antibody. The immunoprecipitated material was eluted with Flag peptide, and re-precipitated with anti-haemagglutinin antibody, after which mass spectrometric analysis was performed. We readily identified Dkk1 and endogenous

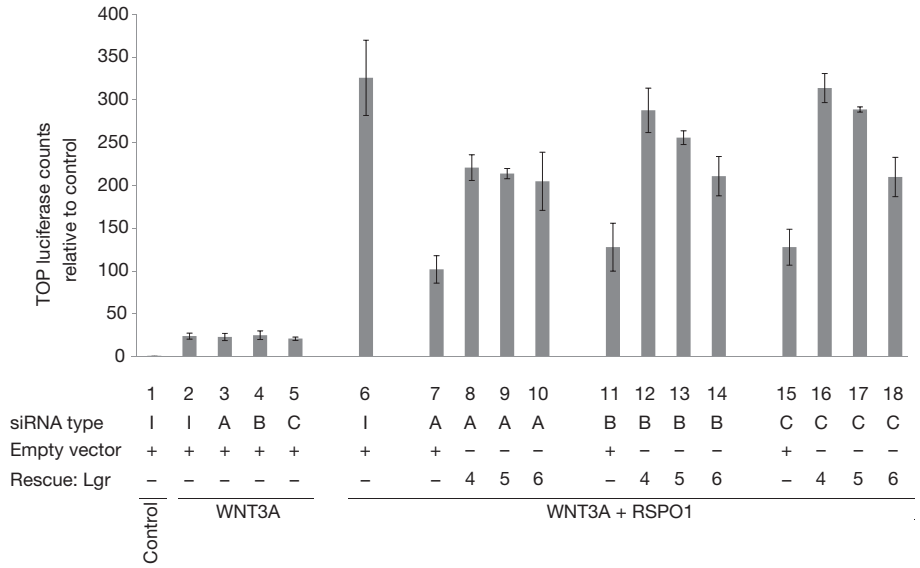

Figure 3 | LGR4 is essential for transmitting RSPO1 signals but dispensable for transmitting WNT3A signals. TOPFLASH Wnt reporter assays. HEK293T cells were transfected with indicated siRNAs. siRNAs A, B, C, siRNAs directed at the 3′UTR of human *LGR4*; siRNA I, pool of scrambled siRNA. Three days later, the cells were transfected with TOPFLASH reporters and 5 ng of the indicated rescue constructs, and incubated with WNT3A and RSPO1 as indicated. WNT3A induced TOPFLASH reporter activity without showing effects of removal of LGR4. R-spondin potentiated the WNT3A response, but this effect was sensitive to removal of LGR4. Rescue was obtained with LGR4, -5, and -6 rescue constructs, but not with control vector (lanes 7, 11, 15). $n = 4$. Error bars indicated as s.d.

LRP5 and LRP6 (Supplementary Table 2). We then produced a double-tagged version of human RSPO1 (RSPO1–FH) at ~1 μg ml^{-1}. As tested in the TOPFLASH WNT reporter assay[31], the protein potentiated the effect of Wnt3A by approximately 12-fold (Fig. 3). We incubated 2×10^9 HEK293 cells with the RSPO1–FH-conditioned medium and subjected them to the above protocol. The only transmembrane protein detected was LGR4 (Supplementary Table 2).

HEK293T cells were transiently transfected with tagged versions of LGR4, LGR5 and LGR6, and with the closely related LGR1 (FSH receptor), LGR3 (TSH receptor), LGR7 and LGR8. Transfected cells were incubated with Fc fusion protein of human RSPO1 at ~1 μg ml^{-1}, washed, lysed and precipitated with protein G beads. Western blotting for the Flag tag revealed binding of RSPO1–Fc to LGR4, LGR5 and LGR6, but not to the other LGR proteins (Fig. 4a). In the same assay, Fc fusion proteins of RSPO2, RSPO3 and RSPO4 at ~1 μg ml^{-1} were shown to bind specifically to LGR4, LGR5 and LGR6 (Supplementary Fig. 4).

Soluble RSPO1–FH interacted with the leucine-rich-repeat exodomain of LGR5 (amino acids 1 to 546) expressed as a human IgG–Fc fusion protein (LGR5-exo–Fc). This allowed surface plasmon resonance array imaging. Anti-Flag antibody, spotted on the sensor chip, captured RSPO1–FH (Fig. 4b, left, blue line). LGR5-exo–Fc bound to RSPO1–FH (left; blue line). After regeneration, a control experiment was performed using a noggin–Fc fusion protein (Fig. 4b, right, blue line), which did not bind RSPO1–FH. Both LGR5-exo–Fc and noggin–Fc could be captured on anti-human IgG spotted as a control (Fig. 4b, red line). The K_D of the LGR5-exo–Fc–RSPO1–FH interaction was determined at 3.1 nM by an extrapolated 1:1 interaction model at serial injections of RSPO1 and LGR5-exo–Fc on anti-Flag spots with decreasing densities (Supplementary Fig. 5). In a dose–response curve in the HEK293T Wnt reporter assay, Wnt signalling was indeed induced by nanomolar amounts of RSPO1 (Supplementary Fig. 6).

Rat monoclonal antibodies were raised against full-length human LGR5 protein. All antibodies reacted with LGR5-exo–Fc and their

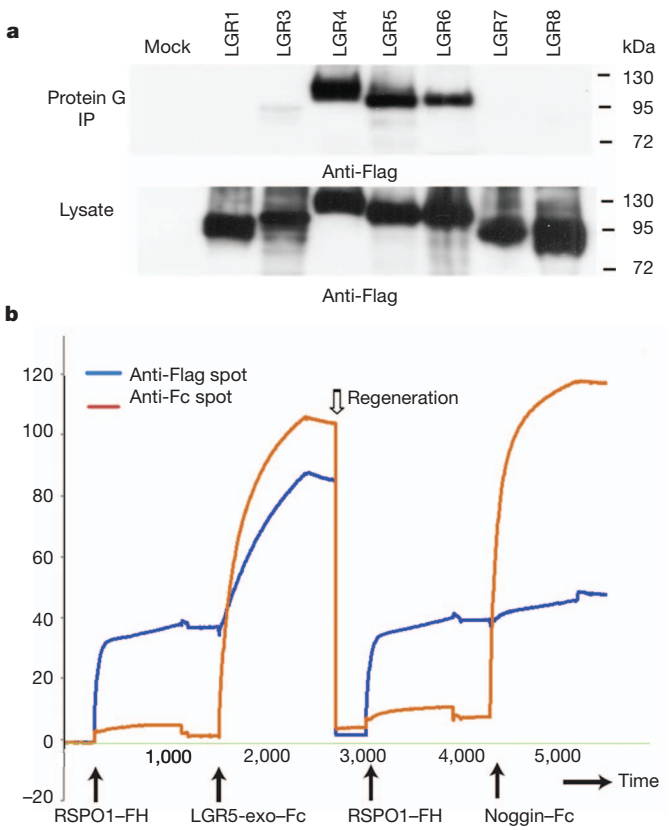

Figure 4 | Direct physical interaction of RSPO1 with LGR4/5/6 exodomains. a, RSPO1 binds to LGR4, LGR5 and LGR6. Top panel, HEK293T cells transfected with Flag-tagged versions of the indicated LGR proteins, incubated with RSPO1–Fc fusion protein at ~1 μg ml^{-1}. Cells were washed, lysed and RSPO1–Fc was immunoprecipitated with protein G beads. Top, western blotting for Flag revealed specific binding to LGR4, LGR5 and LGR6. IP, immunoprecipitation. Bottom, input of tagged proteins. **b**, RSPO1–LGR5 interaction visualized by surface plasmon resonance. Anti-Flag antibody spotted on the sensor chip captured RSPO1–FH (Fig. 4, left, blue line). After a wash, LGR5-exo–Fc bound to RSPO1–FH. After regeneration with low pH, a noggin–Fc fusion protein served as a negative control (Fig. 3, right, blue line). Both LGR5-exo–Fc and noggin–Fc could be captured on goat anti-human IgG spotted as a control (Fig. 3, red line).

epitopes were mapped using carboxy-terminal deletion clones and human-mouse hybrids of the Lgr5 exodomain (Supplementary Fig. 7a). All antibodies recognizing the amino terminus of the Lgr5 extracellular domain blocked the RSPO1 interaction, whereas the other antibodies did not (Supplementary Fig. 7b). Indeed, when the extreme N terminus or the first LRR domain were deleted from Lgr5, RSPO1-binding was lost (Supplementary Fig. 8).

HEK293T cells express *LGR4* but not *LGR5* (Supplementary Fig. 9). To test if LGR4 constitutes a functional RSPO1 receptor, we removed *LGR4* mRNA from HEK293T cells with three independent small interfering RNAs (siRNAs; Supplementary Fig. 9). Subsequently, the cells were transfected with TOPFLASH WNT reporters and their response to exogenously added WNT3A and RSPO1 was measured. WNT3A alone induced a ~25-fold increase in TOPFLASH activity. Removal of LGR4 had no effect on this WNT3A response (Fig. 3; compare bar 1 to bars 2–5). The combination of WNT3A with RSPO1 led to a further ~12-fold increase in TOPFLASH activity (bar 6). This effect was greatly diminished when LGR4 was removed (bars 7, 11 and 15), but could be rescued by transfection of *LGR4* (bars 8, 12 and 16), *LGR5* (bars 9, 13 and 17) or *LGR6* expression plasmids (bars 10, 14 and 18). No rescue was obtained with *LGR1*, *LGR7* or *LGR8* (Supplementary Fig. 10). A 'DRY' motif at the cytosolic end of the third transmembrane region is believed to be essential for protein G coupling in serpentine receptors[32]. We mutated the ERG motif at the corresponding position in LGR5 to ENG. Both versions of LGR5 rescued loss of LGR4 in the TOPFLASH assay (Supplementary Fig. 11), indicating that protein G signalling is not involved in signalling towards β-catenin.

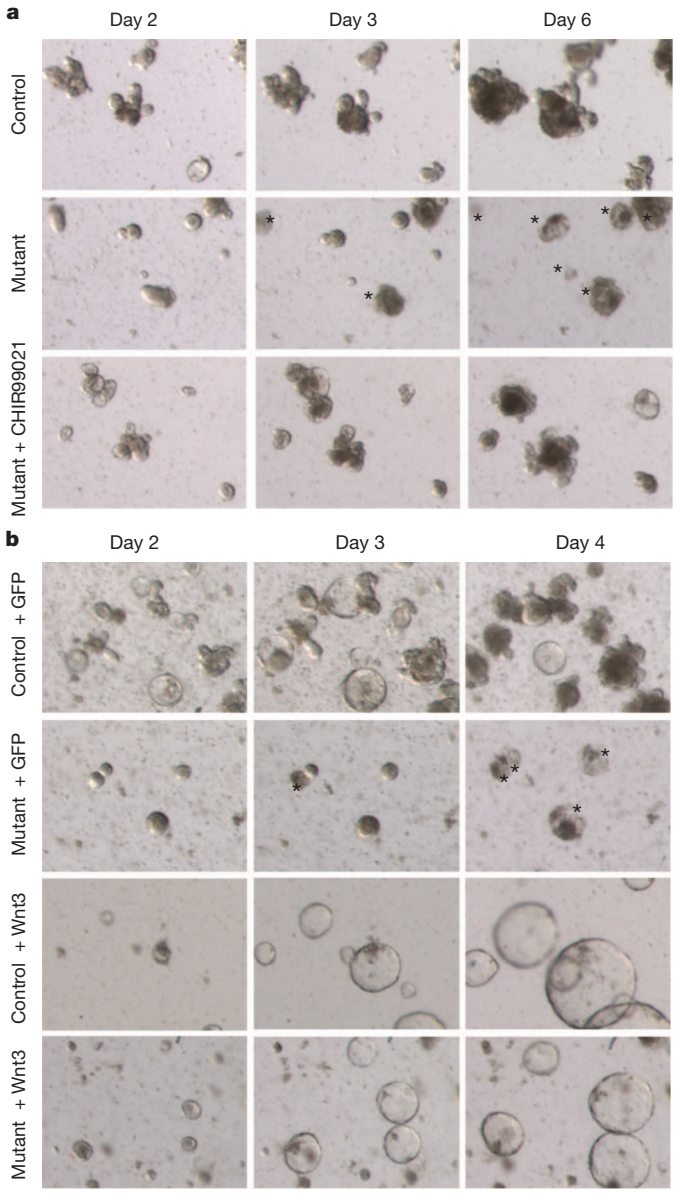

Figure 5 | Rescue of Lgr4/5 deletion in cultured crypt organoids by Wnt signals. a, Organoids established under standard conditions[15] from *Lgr4*$^{fx/fx}$ *Lgr5*$^{fl/fl}$ *Villin-CreERT2* mice[37] (Mutant) or from control *Villin-CreERT2* mice (Control). Tamoxifen treatment leads to death (asterisks) of mutant organoids but not that of controls. This is overcome by addition of CHIR99021 at 5 μM (Mutant + CHIR99021). **b**, Organoids established from *Lgr4*$^{fx/fx}$ *Lgr5*$^{fl/fl}$ *Villin-CreERT2* mice (Mutant) or from control *Villin-CreERT2* mice (Control) are infected with Wnt3-expressing retrovirus, which turns organoids into growing, rounded cysts[34], or with control (GFP) retrovirus. Subsequent deletion of *Lgr4* and *-5* has no effect on Wnt3-expressing organoids but leads to death of control retrovirus organoids.

The proposed model implies that strong Wnt signals should rescue loss of Lgr receptors. We generated intestinal organoids[15] from *Lgr4*$^{fx/fx}$ *Lgr5*$^{fl/fl}$ *Villin-CreERT2* mice. Tamoxifen-induced deletion *in vitro* resulted in the demise of the organoids after 2 days (Fig. 5a). Microarraying was performed 1 day after induction of deletion, that is, 24 h before organoids lost viability. This revealed a striking similarity between gene expression changes 1 day after withdrawal of Rspo1 and 1 day after deletion of the proposed R-spondin receptors Lgr4 and Lgr5 (Fig. 2c and f). Addition of the Gsk3 inhibitor CHIR99021 (which activates the Wnt cascade) led to a quantitative, persistent rescue of *Lgr4/5*-mutant organoids (Supplementary Fig. 12). Of note, LiCl (which inhibits Gsk3, but also inositol monophosphatase[34]) reportedly allows 6% rescue of the growth of *Lgr4*-hypomorphic organoids[7]. We next expressed Wnt3 (ref. 35) by retroviral transduction in established *Lgr4*$^{fx/fx}$ *Lgr5*$^{fl/fl}$ *Villin-CreERT2*. Subsequent tamoxifen-induced deletion of *Lgr4* and *-5* led to the demise of the mutant crypts, but this effect was robustly rescued by Wnt3 overexpression (Fig. 5b). In a similar approach, retrovirally expressed Lgr5 and Lgr5-ENG rescued organoid growth (Supplementary Fig. 13).

These data demonstrate that binding of R-spondins to their cognate receptors, the Lgr5 homologues, triggers downstream canonical Wnt signals through associated frizzled–Lrp5/6 complexes. The current observations assign a crucial function to Lgr4 and Lgr5 in Wnt-dependent stem cells and progenitor cells: in intestinal crypts, Lgr4 and -5, incorporated into frizzled–Lrp complexes, allow R-spondins to augment short-range Wnt signals emanating from Paneth cells[34]. This provides a molecular mechanism for the potent hyperplastic response of crypts to Rspo1 (ref. 24) and will guide future studies towards the application of R-spondins for regenerative purposes of tissues expressing Lgr5 homologues. Moreover, this study reinforces the connection, first described in intestinal crypts[36], between Wnt signalling and adult mammalian stem cell biology.

METHODS SUMMARY

Mice. Experiments were performed according to guidelines and reviewed by the DEC of the KNAW. Knock-in alleles were generated and conditional deletion was induced as described elsewhere[2,13].

Plasmid expression constructs. Available upon request.

Histology. Tissues were prepared and stained with Ki67, PAS, or subjected to fluorescent *in situ* hybridization to *Olfm4* as described elsewhere[13].

Cell culture, transfections, TOPFLASH assays, RSPO1/WNT3A stimulation. HEK293T cells and Ls174T cells were cultured and transfected as described elsewhere[31,36]. siRNAs directed at the 3′ untranslated repeat (3′UTR) of human *LGR4* were from Thermo Scientific Dharmacon. Sense sequences: A, 5′-gaaagua aacuguggucaauu-3′; B, 5′-ggguggagucuuaaaguuauu-3′; C, 5′-gguaagaaacuccu aauuauu-3′; I (irrelevant), ON-TARGETplus Non-Targeting Pool from Dharmacon. Transfected with Dharmafect1.

Microarraying. Performed on an Agilent platform, as described elsewhere[3].

Immunoprecipitation, epitope mapping, western blotting. Performed using standard protocols. Mouse M2 Anti-Flag antibody (Sigma), rabbit anti-human IgG–Fc horse radish peroxidase (HRP) conjugate (Pierce), and goat anti-rat IgG–HRP-conjugate (Pierce) were used. Protein G agarose beads (Millipore).

Mass spectrometric analysis. In all cases, samples were obtained by sequential immunoprecipitation, performed using anti-Flag affinity matrix (Sigma), 3×Flag peptide (Sigma) elution and re-precipitation using anti-haemagglutinin affinity matrix (Roche) as described[21]. For a detailed description of the mass spectrometric analysis see Supplementary Material.

Surface plasmon resonance. Performed by IBIS Technologies, Enschede, The Netherlands.

Rat monoclonal antibodies anti-human LGR5. Generated by Genovac by DNA vaccination with full-length human *LGR5* cDNA. Initial hybridoma screening was performed by fluorescence-activated cell sorting (FACS) on stable human LGR5 transfectants.

Full Methods and any associated references are available in the online version of the paper at www.nature.com/nature.

Received 29 March; accepted 27 June 2011.
Published online 4 July 2011.

1. Barker, N. & Clevers, H. Leucine-rich repeat-containing G-protein-coupled receptors as markers of adult stem cells. *Gastroenterology* **138,** 1681–1696 (2010).
2. Barker, N. *et al.* Identification of stem cells in small intestine and colon by marker gene *Lgr5*. *Nature* **449,** 1003–1007 (2007).
3. Barker, N. *et al.* Lgr5^{+ve} stem cells drive self-renewal in the stomach and build long-lived gastric units *in vitro*. *Cell Stem Cell* **6,** 25–36 (2010).
4. Jaks, V. *et al.* Lgr5 marks cycling, yet long-lived, hair follicle stem cells. *Nature Genet.* **40,** 1291–1299 (2008).
5. Snippert, H. J. *et al. Lgr6* marks stem cells in the hair follicle that generate all cell lineages of the skin. *Science* **327,** 1385–1389 (2010).
6. Van Schoore, G., Mendive, F., Pochet, R. & Vassart, G. Expression pattern of the orphan receptor LGR4/GPR48 gene in the mouse. *Histochem. Cell Biol.* **124,** 35–50 (2005).
7. Mustata, R. C. *et al. Lgr4* is required for Paneth cell differentiation and maintenance of intestinal stem cells I. *EMBO Reports* **12,** 558–564 (2011).
8. van der Flier, L. G. *et al.* Transcription factor achaete scute-like 2 controls intestinal stem cell fate. *Cell* **136,** 903–912 (2009).
9. Morita, H. *et al.* Neonatal lethality of LGR5 null mice is associated with ankyloglossia and gastrointestinal distension. *Mol. Cell. Biol.* **24,** 9736–9743 (2004).
10. Kato, S. *et al.* Eye-open at birth phenotype with reduced keratinocyte motility in LGR4 null mice. *FEBS Lett.* **581,** 4685–4690 (2007).
11. Ireland, H., Houghton, C., Howard, L. & Winton, D. J. Cellular inheritance of a Cre-activated reporter gene to determine Paneth cell longevity in the murine small intestine. *Dev. Dyn.* **233,** 1332–1336 (2005).
12. Garcia, M. I. *et al.* LGR5 deficiency deregulates Wnt signaling and leads to precocious Paneth cell differentiation in the fetal intestine. *Dev. Biol.* **331,** 58–67 (2009).
13. van der Flier, L. G., Haegebarth, A., Stange, D. E., van de Wetering, M. & Clevers, H. OLFM4 is a robust marker for stem cells in human intestine and marks a subset of colorectal cancer cells. *Gastroenterology* **137,** 15–17 (2009).
14. Muncan, V. *et al.* Rapid loss of intestinal crypts upon conditional deletion of the Wnt/Tcf-4 target gene c-*Myc*. *Mol. Cell. Biol.* **26,** 8418–8426 (2006).
15. Sato, T. *et al.* Single Lgr5 stem cells build crypt-villus structures *in vitro* without a mesenchymal niche. *Nature* **459,** 262–265 (2009).
16. Pinto, D., Gregorieff, A., Begthel, H. & Clevers, H. Canonical Wnt signals are essential for homeostasis of the intestinal epithelium. *Genes Dev.* **17,** 1709–1713 (2003).
17. Kuhnert, F. *et al.* Essential requirement for Wnt signaling in proliferation of adult small intestine and colon revealed by adenoviral expression of Dickkopf-1. *Proc. Natl Acad. Sci. USA* **101,** 266–271 (2004).
18. van Es, J. H. *et al.* Notch/γ-secretase inhibition turns proliferative cells in intestinal crypts and adenomas into goblet cells. *Nature* **435,** 959–963 (2005).
19. Sansom, O. J. *et al. Myc* deletion rescues Apc deficiency in the small intestine. *Nature* **446,** 676–679 (2007).
20. Subramanian, A. *et al.* Gene set enrichment analysis: a knowledge-based approach for interpreting genome-wide expression profiles. *Proc. Natl Acad. Sci. USA* **102,** 15545–15550 (2005).
21. Nakatani, Y. & Ogryzko, V. Immunoaffinity purification of mammalian protein complexes. *Methods Enzymol.* **370,** 430–444 (2003).
22. Kazanskaya, O. *et al.* R-Spondin2 is a secreted activator of Wnt/β-catenin signaling and is required for *Xenopus* myogenesis. *Dev. Cell* **7,** 525–534 (2004).
23. Kim, K. A. *et al.* R-spondin family members regulate the Wnt pathway by a common mechanism. *Mol. Biol. Cell* **19,** 2588–2596 (2008).
24. Kim, K. A. *et al.* Mitogenic influence of human R-spondin1 on the intestinal epithelium. *Science* **309,** 1256–1259 (2005).
25. Zhao, J. *et al.* R-spondin1, a novel intestinotrophic mitogen, ameliorates experimental colitis in mice. *Gastroenterology* **132,** 1331–1343 (2007).
26. Ohkawara, B., Glinka, A. & Niehrs, C. Rspo3 binds syndecan 4 and induces Wnt/PCP signaling via clathrin-mediated endocytosis to promote morphogenesis. *Dev. Cell* **20,** 303–314 (2011).
27. Nam, J. S., Turcotte, T. J., Smith, P. F., Choi, S. & Yoon, J. K. Mouse cristin/R-spondin family proteins are novel ligands for the Frizzled 8 and LRP6 receptors and activate β-catenin-dependent gene expression. *J. Biol. Chem.* **281,** 13247–13257 (2006).
28. Wei, Q. *et al.* R-spondin1 is a high affinity ligand for LRP6 and induces LRP6 phosphorylation and β-catenin signaling. *J. Biol. Chem.* **282,** 15903–15911 (2007).
29. Binnerts, M. E. *et al.* R-Spondin1 regulates Wnt signaling by inhibiting internalization of LRP6. *Proc. Natl Acad. Sci. USA* **104,** 14700–14705 (2007).
30. Glinka, A. *et al.* Dickkopf-1 is a member of a new family of secreted proteins and functions in head induction. *Nature* **391,** 357–362 (1998).
31. Korinek, V. *et al.* Constitutive transcriptional activation by a β-catenin-Tcf complex in APC$^{-/-}$ colon carcinoma. *Science* **275,** 1784–1787 (1997).
32. Flanagan, C. A. A. GPCR that is not "DRY". *Mol. Pharmacol.* **68,** 1–3 (2005).
33. Robine, S., Sahuquillo-Merino, C., Louvard, D. & Pringault, E. Regulatory sequences on the human villin gene trigger the expression of a reporter gene in a differentiating HT29 intestinal cell line. *J. Biol. Chem.* **268,** 11426–11434 (1993).
34. Klein, P. S. & Melton, D. A. A molecular mechanism for the effect of lithium on development. *Proc. Natl Acad. Sci. USA* **93,** 8455–8459 (1996).
35. Sato, T. *et al.* Paneth cells constitute the niche for Lgr5 stem cells in intestinal crypts. *Nature* **469,** 415–418 (2011).
36. Korinek, V. *et al.* Depletion of epithelial stem-cell compartments in the small intestine of mice lacking Tcf-4. *Nature Genet.* **19,** 379–383 (1998).
37. Ng, S. S. *et al.* Phosphatidylinositol 3-kinase signaling does not activate the Wnt cascade. *J. Biol. Chem.* **284,** 35308–35313 (2009).

Supplementary Information is linked to the online version of the paper at www.nature.com/nature.

Acknowledgements We thank G. Vassart for *Lgr4-LacZ* intestinal tissue, D. Winton for *Ah-Cre* mice, S. Robine for *Villin-CreERT2* mice, A. Moerkamp and C. Verheul for experimental help and H. Farin for figures.

Author Contributions All Hubrecht Institute authors performed experiments under guidance of H.C.; S.M., A.J.R.H. and T.Y.L. performed mass spectrometry; P.K. and P.J.P. performed electron microscopy analysis; R.B.M.S. performed plasmon surface resonance; and Y.M. and K.N. generated the *Lgr4* knockout mouse.

Author Information Microarray data have been deposited in the GEO database under accession number GSE28265. Mass spectrometry data sets are available at ProteomeCommons.org Tranche Repository https://proteomecommons.org/tranche/data-downloader.jsp?h=2LOW5tCJBOfT%2FpcCAtMrPqCgTTOd247s6poPgSvwu16KiVwCfExWdJ0jifGdI4FraidTHUnI1PYhloT0nTs1zdwKmKEAAAAAAACzw%3D%3D. Reprints and permissions information is available at www.nature.com/reprints. The authors declare competing financial interests: details accompany the full-text HTML version of the paper at www.nature.com/nature. Readers are welcome to comment on the online version of this article at www.nature.com/nature. Correspondence and requests for materials should be addressed to H.C. (h.clevers@hubrecht.eu).

METHODS

Microarray analysis *Lgr4/5* knockout mice. Small intestinal crypts were isolated 1 day after induction of deletion from *AHCre Lgr4fx/fx Lgr5fl/fl* as well as wild-type mice by incubation in 2 mM EDTA, RNA was isolated using TRIzol (Invitrogen) and 1 μg of RNA was labelled using a Quick Amp Labelling Kit, two colour (Agilent Technologies) with Cy5 and Cy3, respectively; all as described elsewhere[3]. Two separate biological replicates were performed in dye-swap, resulting in four individual arrays. Labelling, hybridization and washing were done according to Agilent guidelines. Differentially labelled cRNA was hybridized on 4X44K Agilent Whole Mouse Genome dual colour Microarrays (G4122F). Array data were normalized and retrieved using Feature Extraction (V.9.5.3, Agilent Technologies) and data analyses were performed using Microsoft Excel (Microsoft Corporation). Features were flagged, if signal intensities for both the Cy3 and Cy5 channel did not pass the feature extraction filter, 'significant and positive' or 'well above background'. Genes were considered downregulated if 4 out of 4 arrays showed a significant ($P < 0.05$) downregulation of < -0.58 (linear -1.5 fold). This resulted in 379 entries, which 307 unique genes (Supplementary Table array data will be available at the Gene Expression Omnibus http://www.ncbi.nlm.nih.gov/geo).

R-spondin1 withdrawal in mouse intestinal organoids. Crypts were isolated from a wild-type mouse small intestine by incubating with 2 mM EDTA in PBS for 30 min at 4 °C, and subsequently grown in crypt culture medium as reported previously[16]. Briefly, isolated crypts were cultured in Matrigel (BD Bioscience) in 24-well plates, and advanced DMEM/F12 medium (Invitrogen) containing epithelial growth factor, noggin and Rspo1 was added after polymerization of Matrigel. Confluent organoids were split into multiple wells, and were then cultured in crypt culture medium in the presence or absence of Rspo1. One day after Rspo1 withdrawal organoids (−RSpo1 organoids) and the control organoids (+Rspo1 organoids) were then collected for RNA extraction and microarray analysis. RNA from control and Rspo1 depleted organoids (1 μg), together with universal mouse reference RNA (Stratagene), was labelled using a Quick Amp Labelling Kit, two colour (Agilent Technologies) with Cy5 and Cy3, respectively. Samples were hybridized to 4X44K Whole Mouse Genome Microarrays (Agilent, G4122F) according to manufacturer's instructions. Microarray signal and background information were retrieved and normalized using the Feature Extraction program (V.9.5.3, Agilent Technologies). Samples were considered as well-measured when the fluorescent signals in red channel (Cy5) in either of the samples were greater than twofold above the local background. Differences between −Rspo1 organoids and +Rspo1 organoids were calculated by subtracting the ratio for '−Rspo1 organoids versus reference RNA' from '+Rspo1 versus reference RNA'. Array data is available at the Gene Expression Omnibus (http://www.ncbi.nlm.nih.gov/geo).

Heat map and gene set enrichment analysis. Heat maps were generated using MeV (Multiple Experiment Viewer v.4.3)[42]. Heat maps were generated using the 306 genes from the *Lgr4/5* gene set and plotting the ratios of two different experiments for these genes. Figure 2a contains the ratios from ref. 15, where the authors deleted *Apc* in the *Ah-Cre* $Apc^{fl/fl}$ mice and performed microarray analysis 3 days after deletion. Figure 2b contains the ratios form the Rspo1 withdrawal experiment described above. Gene set enrichment analysis (GSEA) implemented with GSEAP v.2.0 (http://www.broad.mit.edu/gsea) was used to identify significant enrichments of the *Lgr4/5* gene set in the two different experimental scenarios mentioned above. All 'well measured' features ($n = 20{,}844$) for the Rspo1 experiment from the Agilent arrays and all features with a ratio ($n = 45{,}101$) for the *Apc* arrays from the Affymetrix platform were used for the ranked gene list in GSEA.

Mass spectrometric analysis. The samples were subjected to SDS–PAGE followed by Coomassie blue staining. The gel lane was sliced into 24 equal sections and digested. In brief, protein reduction and alkylation was performed with dithiothreitol (60 °C, 1 h) and iodoacetamide (dark, room temperature, 30 min), respectively. Digestion was performed with trypsin overnight at 37 °C. Peptides were extracted with 10% formic acid[38].

The extracted peptides were subjected to nanoscale liquid chromatography tandem mass spectrometry (nanoLC-MS/MS) analysis, performed on an Agilent 1200 HPLC system (Agilent technologies) connected to an LTQ Orbitrap Velos (ThermoFisher)[39]. The nanoLC was equipped with a 20 mm × 100 μm internal diameter trap column and a 400 mm × 50 μm internal diameter analytical column (Reprosil C18, Dr Maisch). Trapping was performed at a flow of 5 μl min^{-1} for 10 min and the fractions were eluted using a 45 min linear gradient from 0 to 40% solvent B (0.1 M acetic acid in 80% acetonitrile (v/v), in which solvent A was 0.1 M acetic acid), 40 to 100% solvent B in 2 min and 100% B for 2.5 min. The analytical flow rate was 100 nl min^{-1} and the column effluent was directly introduced into the electrospray source of the mass spectrometer using a standard coated fused silica emitter (New Objective) (outer diameter 360 μm, tip internal diameter 10 μm) biased to 1.7 kV. The mass spectrometer was operated in positive ion mode and in data-dependent mode to automatically switch between MS and MS/MS. The five most intense ions in the survey scan were fragmented in the linear ion trap using collision-induced dissociation[40]. The target ion setting was 5×10^5 for the Orbitrap, with a maximum fill-time of 250 ms. Fragment ion spectra were acquired in the LTQ with an automatic gain control value of 5×10^3 and a max injection time of 100 ms.

Protein identification: raw mass spectrometry data were converted to peak lists using MaxQuant version 1.0.13.13 (ref. 41). Spectra were searched against the IPI (International Protein Index) Human database version 3.37 (69,164 sequences; 29,064,824 residues) using the Mascot search engine (version 2.3.02; http://www.matrixscience.com), with trypsin set as enzyme. The database search was made with the following parameters set to consider a peptide tolerance of ±15 p.p.m., a fragment tolerance of ±0.5 Da, allowing two missed cleavages, carbamidomethyl (C) as fixed modification; oxidation (M) and protein N-terminal acetylation as variable modifications.

Plasmon surface resonance. A pre-activated ester sensor chip (IBIS Technologies) was spotted using a Continuous Flow Microspotter (Wasatch Microfluidics). In total, 32 spots were created with both mouse anti-Flag and goat anti-human IgG in 8× serial dilution (start concentrations were 500 μg ml^{-1} and 100 μg ml^{-1}, respectively) in 10 mM MES buffer pH 5.5. Control (reference) spots contained human serum albumin, anti-human serum albumin and MES buffer. After preparing the sensor chip, the slider was positioned in an IBIS MX96 (IBIS Technologies) for label-free surface plasmon resonance (SPR) array analysis. The instrument enables multiplex interactions up to 96-plex using scanning imaging optics for automated calculation of the SPR dip shifts of all region of interests simultaneously. The signal-to-noise ratio of the instrument which reflects the limit of detection is better than 1 RU corresponding to 1 picogram protein per square millimetre. In the IBIS MX96, back and forth mixing is applied enabling minimal use of sample while the length of the exposure of the sample to the microarray is unlimited and not affected by the volume of, for example, an injection loop. A two-step interaction process was carried out and the multiplex interaction event to all spots of the array was recorded simultaneously. In this way, chip-to-chip and sample-to-sample variations can be excluded, while positive and negative controls and referencing can be applied instantly. A microscope image of the sensor chip (not shown here) can reveal any irregularities, heterogeneities of the spots and/or disturbing air bubbles. First 70 μl of RSPO1–FH was injected followed by dissociation and second injection of 70 μl LGR5–Fc. After regeneration with acid buffer (Gly-HCl, 10 mM, pH 2.0) for 120 s, the control experiment was capture of RSPO1–FH followed by injection of noggin–Fc (results see Fig. 4b). For affinity constant determination first RSPO1–FH was captured on the anti-Flag spot until saturation of the spot followed by injection of LGR5–Fc (8 μg ml^{-1}). RSPO1 was not immobilized directly on the chip because it did not survive the acid regeneration process (data not shown). Capturing of RSPO1–FH was possible on the anti-Flag antibody spot from growth medium. Supplementary Fig. 1 is an overlay plot of three interaction series of first RSPO1–FH (2 min association was sufficient to reach saturation) and three different concentrations of LGR5–Fc (molecular mass 176 kDa) corresponding to 45 nM, 23 nM and 11 nM injections. Referencing was carried out by subtraction of the anti-Flag spot signal with the signal coming from a HAS-loaded spot in SPRint software (IBIS Technologies) for compensating bulk refractive index shifts for example, as a result of growth medium compounds. The affinity constant was calculated using a discrete 1:1 interaction model using global fitting (Scrubber 2, BioLogic Software Pty Ltd). In Supplementary Fig. 1, the residual plot of the experimental curve minus fit values is shown and although it cannot be revealed that the interaction process is according to a discrete 1:1 interaction model the affinity constant was calculated to be ~3 nM. It was not necessary to add an extra fit parameter for mass transport limitation compensation, due to a high back and forth mixing condition in the IBIS MX96 flow cell.

38. Shevchenko, A., Wilm, M., Vorm, O. & Mann, M. Mass spectrometric sequencing of proteins silver-stained polyacrylamide gels. *Anal. Chem.* **68,** 850–858 (1996).
39. Raijmakers, R. *et al.* Automated online sequential isotope labeling for protein quantitation applied to proteasome tissue-specific diversity. *Mol. Cell. Proteomics* **7,** 1755–1762 (2008).
40. Frese, C. K. *et al.* Improved peptide identification by targeted fragmentation using CID, HCD and ETD on a LTQ-Orbitrap Velos. *J. Proteome Res.* **10,** 2377–2388 (2011).
41. Cox, J. & Mann, M. MaxQuant enables high peptide identification rates, individualized p.p.b.-range mass accuracies and proteome-wide protein quantification. *Nature Biotechnol.* **26,** 1367–1372 (2008).
42. Saeed, A. I. *et al.* TM4: a free, open-source system for microarray data management and analysis. Biotechniques, **34,** 374–378 (2003).